Chemical Engineering Journal 414 (2021) 128694

Contents lists available at ScienceDirect

Chemical Engineering Journal

journal homepage: www.elsevier.com/locate/cej

How to adjust bubble's adhesion on solid in aqueous media: Femtosecond laser-ablated patterned shape-memory polymer surfaces to achieve bubble multi-manipulation

Jinglan Huo [a], Xue Bai [a], Jiale Yong [a], Yao Fang [a], Qing Yang [b,*], Xun Hou [a,b], Feng Chen [a,*]

[a] State Key Laboratory for Manufacturing System Engineering and Shaanxi Key Laboratory of Photonics Technology for Information, School of Electronic Science and Engineering, Xi'an Jiaotong University, Xi'an 710049, PR China
[b] School of Mechanical Engineering, Xi'an Jiaotong University, Xi'an 710049, PR China

ARTICLE INFO

Keywords:
Adjustable bubble adhesion
Bubble multi-manipulation
Femtosecond laser
Shape-memory polymer

ABSTRACT

Manipulation of the behaviour of gas bubbles in aqueous environment is of vital significance in medical and microfluidic fields, and has attracted much research attention in the past few years. Making clear the interrelation between underwater bubbles' wettability and the solid surfaces topography to achieve the bubble adhesion regulation is a crucial factor of realizing the precise bubble manipulation without external stimulation, and a great challenge. Here, by combining the fish-scale-like morphology and rose-petal-like morphology into one sample and changing the proportion of each part, the underwater bubble adhesion could be adjusted from ultralow to low, high, and ultrahigh. The square-patterned array shape-memory polymer (SMP) surfaces with various adhesion forces were fabricated by femtosecond laser ablation and used to realize lossless transportation of a bubble in both horizontal and vertical direction. The high adhesion surface could be used to form programmable microbubble patterns. By taking advantage of the excellent thermal shape-memory character of SMP film, we realized the bubble in-situ release and reversely switch of the bubble adhesion based on the macroscopic and microscopic deforming-recovering of as-prepared SMP sample. The present study will inspire people to develop novel strategies to achieve multi-manipulation of bubbles in practical applications.

1. Introduction

Controlling gas bubbles in aqueous environment is of great significance in medical field, microfluidics field and undersea detection, such as drug delivery [1–3], three-dimension (3D) porous polymer fabrication [4–6], underwater acoustic enhancement [7] and so on. Figuring out the interaction between bubbles and solid surfaces in water is the key factor of underwater bubble manipulation [8–15]. The behaviour of bubbles on a solid surface is mainly affected by the bubbles' own buoyancy, external traction force (Laplace force, surface tension difference, magnetic force), and adhesion force [16–30]. Until now, the researchers have realized the control of underwater bubbles from the first two aspects. Jiang et al. designed the underwater superaerophilic helix structure to manipulate air bubbles [16]. Once rotating the helix structure, bubbles always tended to stay on the summit of every helix by the resultant force of buoyancy, traction and adherence. Hence, bubbles moved directionally along with the vertical direction to rotary surface while the helix structure constantly rotating. Yu et al. fabricated a kind of superaerophilic copper cones via electro-etching from Copper wires with diameter of 1.0 mm [17]. The copper cones could be utilized to transport gas bubbles from the tips point to the base point spontaneously and directionally driving by gradient of Laplace pressure of the conical morphology. Ma et al. reported a superaerophilic trapezia-shape polyethylene (*PE*) surface by the techniques of CO_2-laser cutting and low surface energy substance coating [18]. This surface could capture gas bubbles and transported them from small side to large side owning to the shape-gradient morphology and low hysteresis resistance force. Wu et al. controlled the sliding and pinning of bubbles on lubricant-infused porous surface (SLIPS) through optothermal response and magnetism response strategies [19,20]. Oil film on the slippery SLIPS markedly decrease the roughness of the solid surface thereby reducing its friction force and contact angle hysteresis of bubbles. However, those manipulations all based on the ultrahigh adhesion surfaces and suffered the shortcomings of either only 1D unidirectional movement and short

* Corresponding authors.
E-mail addresses: yangqing@mail.xjtu.edu.cn (Q. Yang), chenfeng@mail.xjtu.edu.cn (F. Chen).

https://doi.org/10.1016/j.cej.2021.128694
Received 30 September 2020; Received in revised form 7 January 2021; Accepted 22 January 2021
Available online 27 January 2021

action distance, or only operating on one sample. The adhesion force between a bubble and the solid surface directly affects the bubble's behavior on the solid surface. Enabling to make the bubble adhesion of the solid more adjustable except for the traditional ultralow and ultrahigh adhesion, the bubbles' manipulation will be more flexible, which is difficult to realize due to the high requirement for the surface topography, and rarely reported.

The fish scale with micro/nanoscale protrusions and high free energy possesses underwater superaerophobicity and ultralow bubble adhesion, while the rose petal with only micropapilla structure and high free energy is endowed with underwater aerophobicity and ultrahigh bubble adhesion [8,31]. Combining the two type surfaces and adjusting the proportion of each part to change the bubble/solid contact state to control the bubbles' adhesion is a feasible program. Femtosecond laser ablation has been proved to be one of the most effective methods to construct the surface morphology due to the ultra-short pulse width and extremely high peak power [32,33]. Those features endow the femtosecond laser with "cold working" property for elaborate processing on nearly all of the known materials through one-step ablation process [34–36].

Herein, we designed the rough square-patterned array on intrinsic aerophobic and high-adhesive solid surface by femtosecond laser ablation to realize the adjusted bubble's adhesion force on solid and figure out the relationship between the solid structure pattern and its adhesion force to bubble. SMP is a kind of stimuli-responsive material that can recover to its original shape from temporary shape under external stimulation [37–41]. The solid tested in this experiment was the thermal-response SMP film. The thermal-response SMP surface has been used as a kind of smart surface to realize water reversible wettability transition under thermal treatment and pressing processing [39–41]. On the laser-structured SMP film, the bubble sliding angle (*BSA*) could be adjusted from ultralow to ultrahigh. Utilizing the samples with various adhesion, the air bubble was losslessly transported from one piece to another both in horizontal and vertical direction. The sample with specific adhesion could be used to split microbubbles from a "big" bubble and form the rewritable microbubble pattern freely. The pattern was easy to be erased and rewrited again. In addition, by taking advantages of the microscopic and macroscopic shape-memory characteristic of the SMP film, the controllable in-situ bubble release and reverse bubble adhesion transition were realized. We believe the multi-manipulation of underwater bubble based on the solid's bubble adhesion variation will provide a potential in future applications.

2. Experimental

2.1. Preparation of SMP film

The liquid SMP was obtained by mixing the diglycidyl ether of bisphenol A (DGEBA, SMP prepolymer, Nantong Xingchen Synthetic Material Co., Ltd), n-octylamine (OA, J&K Scientific Ltd) and m-xylylenediamine (MXDA, J&K Scientific Ltd) with the molar ratio of 5:1:2 in a glass beaker. Stirring the polymer mixture for 5 min to make it thoroughly mix for better crosslinking later. Afterwards, the beaker with mixture was placed in a vacuum chamber to remove the needless bubble. Then the degassed SMP liquid polymer was poured into smooth PTFE mold. The mold filled with SMP polymer was moved into heating chamber and cured at 60° for 2 h and 100° for 1 h. Finally, the SMP film was obtained by peeling from the PTFE mold.

2.2. Surface femtosecond laser irradiation

A regenerative amplified Ti: sapphire laser system (Libra-usp-he, Coherent, American) with the pulse duration, central wavelength, and repetition rate of 50 fs, 800 nm, and 1 kHz was used. For the formation of square-patterned array, the laser beam was focused onto the sample through a microscope objective lens (10×, NA = 0.30, Nikon, Japan). The pulse energy was adjusted by apertures and a neutral density attenuator. The "line-by-line" scanning route was used to construct microstructures on sample surface. The value of the laser power, the scanning speed and the interval of scanning lines in the formation of square-patterned array are 20 mW, 6 mm/s, and 6 μm, respectively. For the formation of micro-cone array, the laser beam was focused onto the sample through an optical lens with focus of 200 mm. The value of the laser power, the scanning speed and the interval of scanning lines in the formation of micro-cone array are 250 mW, 3 mm/s, and 100 μm, respectively.

2.3. Characteristics

The two-dimension (2D) morphology of femtosecond laser-structured SMP surface was obtained by a FlexSEM-1000 scanning electron microscope (SEM, Hitachi, Japan). The three-dimention (3D) morphology of hierachical rough SMP surface was characterized by a LEXT-OLS4000 laser confocal microscope (Olympus, Japan). The underwater bubble contact angles and bubble sliding angles were measured by a JC2000D contact-angle system (Powereach, China).

3. Results and discussion

3.1. Morphology and wettability of the smooth and rough SMP surface

Fig. 1 shows the SEM images and underwater bubble wettability on the femtosecond laser-structured and planar SMP surface. The surface of planar SMP is smooth without any particles covering. Once being immersed into water facedown, a 7 μL air bubble could pin on the planar SMP surface with underwater bubble contact angle (*BCA*) of 118°, presenting that it is intrinsic underwater aerophobic and has high bubble adhesion force (Fig. 1a). When turning the planar SMP surface over or upright, the bubble still pinned on (Fig. S1). Femtosecond laser is an effective means of surface modification owning to its tiny light spot, small thermal effect, and high-precision machining [32,33]. After the femtosecond laser directly writing on the SMP surface through "line-by-line" scanning method, the surface material of scanning area was recasted to form the hierarchical structures. The hierarchical structures consist of plenty of microscale protrusions with size of 1 μm to 5 μm and nanoscale swelling with size of 300 nm to 400 nm decorated on the micro-protrusions (Fig. 1b). The wettability of a water droplet on the planar and structured SMP surface are shown in Fig. S1. According the underwater vision of Cassie equation, with increasing of the surface roughness, the underwater *BCA* of the solid/liquid compound surface would correspondingly increase [42]. Once a 7 μL air bubble was placed onto the laser-structured SMP surface, it retained an intact sphere shape with the underwater *BCA* of 160° (inset image in Fig. 1b). Slightly tilted the sample surface with the angle of 3°, the air bubble rolling away rapidly (Fig. 1c). Hence, laser modification endowed the SMP surface with underwater superaerophobicity and ultralow bubble adhesion force. If adjusting the structured low-adhesion area fraction in the planar high-adhesion surface, the bubble's adhesion force of the SMP surface is speculated being adjusted.

3.2. Bubble adhesion adjusting on femtosecond laser-textured SMP surface

Fig. 2a shows the schematic illustration of fabricating the square-patterned array on SMP surface by femtosecond laser directly writing. The line-by-line scanning method was used to generate the rough square-patterned array. The length (*L*) of the structured square side and distance (*D*) between the two square sides adjacent to each other could be adjusted to change the area proportions of planar domain and structured domain and thus determined the underwater bubble adhesion of the as-prepared SMP film. Fig. 2b exhibited the SEM image of the laser-structured square-patterned array with designed *L* of 50 μm and *D*

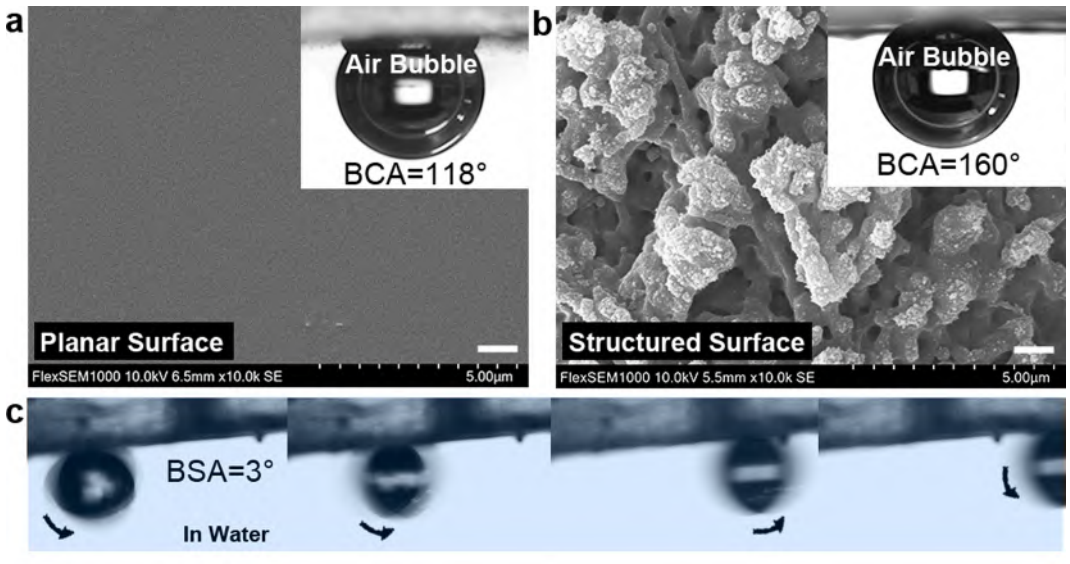

Fig. 1. SEM images of planar SMP surface (a) and laser-structured SMP surface (b). The inset in (a) and (b) shows the *BCA* on the relevant surface. (c) The photo sequence of bubble rolling along the laser-structured SMP surface. The scale bars in (a) and (b) are 1 μm.

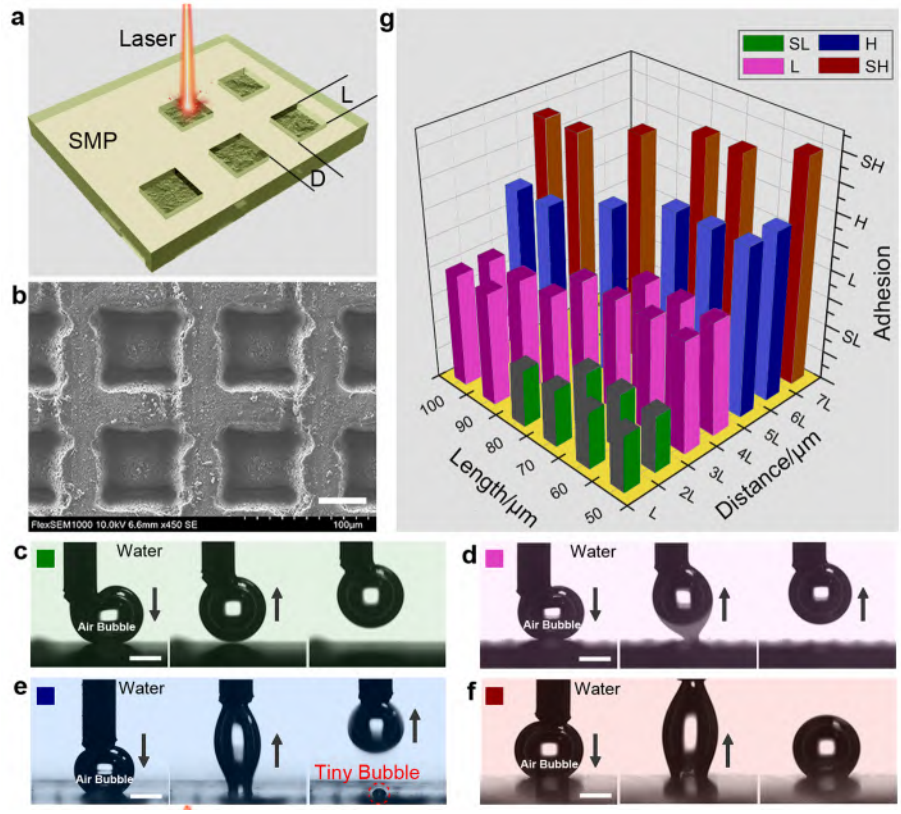

Fig. 2. The results of bubble behaviors on the laser-textured SMP surfaces with different diameters. (a) Schematic depiction of the formation of square-patterned array by femtosecond laser ablation on SMP film. (b) SEM image of 50/50-patterned array SMP film. (c-d) The definition of underwater bubble adhesion *(SLA, LA, HA, SHA)* on solid surfaces. (g) The bubble adhesion on the as-prepared SMP surface with different *L* and *D*. The scale bars in (b) and (c–f) are 40 μm and 500 μm.

of 50 μm. Because of the focusing spot diameter of 10 μm and the molten-recasting effect of laser processing, the real value of *L* and *D* were about 60 μm and 30 μm, respectively. The structuring depth is measured to be 33.81 μm shown in Fig. S2. The structured domain showed micro/nanoscale hierarchical structures as expected while several nano-structures piled up on planar domain (Fig. S3). The resulted samples are referred as *L/D*-patterned surface in the following text.

To show how the underwater bubble adhesion force varies getting rid of the influence of underwater buoyancy, the press-lifting method was used to evaluate the bubble's adhesion on the sample surface. A 0.5 μL microbubble was squeezed by the microinjection, contacted with the sample surface, and then lifted up by the microinjection. To thoroughly contact with the sample and overcome the interference of the enveloped liquid membrane, the microbubble was pressed on the surface for 3 s

before being lifted up. Summarizing from the measuring results on all the as-prepared samples, we concluded four types of adhesion states between the microbubble and samples when lifting up the bubble. For the first state, when the bubble was pressed, its deformation was not very obvious, and was easy to depart from the surface. We defined this kind of surface as super-low-adhesion (*SLA*) surface (Fig. 2c). As for the second state, after press-lifting process, the microbubble was dragged by the surface and then detached from it without any bubble residual (Fig. 2d). This kind of surface was defined as low-adhesion (*LA*) surface. In the third state, when the bubble was lifted up from the surface by microinjection, it was dragged and deformed at the contact point. A tiny bubble left on the contact point after the bubble depart from the surface due to the surface adhesion. We defined this kind of surface as high-adhesion (*HA*) surface (Fig. 2e). At last, if the bubble was pulled down and sit on the surface after press-lifting process, the surface was regarded as a super-high-adhesion (*SHA*) surface with ultrahigh underwater bubble adhesion (Fig. 2f).

According to the adhesion definition concluded above, the 50/50-patterned surface was measured to be the *SLA* surface (Fig. 2b). While increasing the value of *D* to 2*L*, 3*L*, 4*L*, 5*L*, 6*L*, 7*L*, that is 100 μm, 150 μm, 200 μm, 250 μm, 300 μm, 350 μm, the planar domain proportion increased (Fig. S1), and the surface bubble adhesion varied from *SLA* to *SHA* (Fig. 2g). The result revealed that the underwater bubble adhesion on the SMP surface could be adjusted during $D = 2L$ to $D = 7L$ when $L =$ 50 μm. Similarly, while increasing the superaerophobic structured domain area ($L =$ 60 μm, 70 μm, 80 μm, 90 μm, 100 μm) and corresponding planar domain area (determined by *D*), the bubble adhesion on the square-patterned SMP surface could also be adjusted in different scopes (Fig. 2g).

The dynamic underwater bubble behavior that can directly characterize the surface adhesion on the square-patterned SMP surface was demonstrated in Fig. 3a. The as-prepared samples were fixed in the reservoir facedown, and then the reservoir was filled with water. A 7 μL bubble was released below and then contacted the samples under the action of buoyancy. Afterwards, seal the upper opening of the reservoir and rotate the whole reservoir to observe the *BSA* of square-patterned surface with different parameters. Taking the case of *L* equaled to 80 μm, the *BSA* could vary with the change of *D*. When *D* equaled to 160 μm, the underwater bubble would roll away along the 80/160-patterned surface easily when the surface was tilted only a small angle below 2°. If *D* ranged from 160 μm to 260 μm, the *BSA* curve increased sharply from 2° to 90°, indicating that the bubble adhesion of the processed square-patterned SMP surface was adjusted in this scope. When *D* equaled to 260 μm and more, the bubble could pin on the surfaces even when the surfaces were upright or upside down. To verify the conjecture that the adjustment of bubble adhesion on the square-patterned surface fabricated by femtosecond laser is applicative on different material, the stainless steel mesh (*SSM*) was chosen to take a test. It has already been proved that the original *SSM* is underwater aerophobic with ultrahigh adhesion and the laser-structured *SSM* is underwater superaerophobic with ultralow adhesion [43]. Hence, when *L* was set as 80 μm, by changing the *D* from 160 μm to 400 μm, the *BSA* of *SSM* could be successfully controlled from 0° to 90°. It is well known that the femtosecond laser could theoretically process almost all of the solid materials including metals, semiconductors, and polymers due to its extremely high peak power. Therefore, we speculated that femtosecond laser-ablated square-patterned array surface could realize the control of underwater bubble adhesion from ultralow to ultrahigh on nearly any intrinsic aerophobic material. The specific adjustment on the various materials is depended on the value of surface energy. We also explored the effect of depth of the square rough regions (using 80/280-patterned SMP sample), volume of the gas bubble (using 80/260-patterned SMP

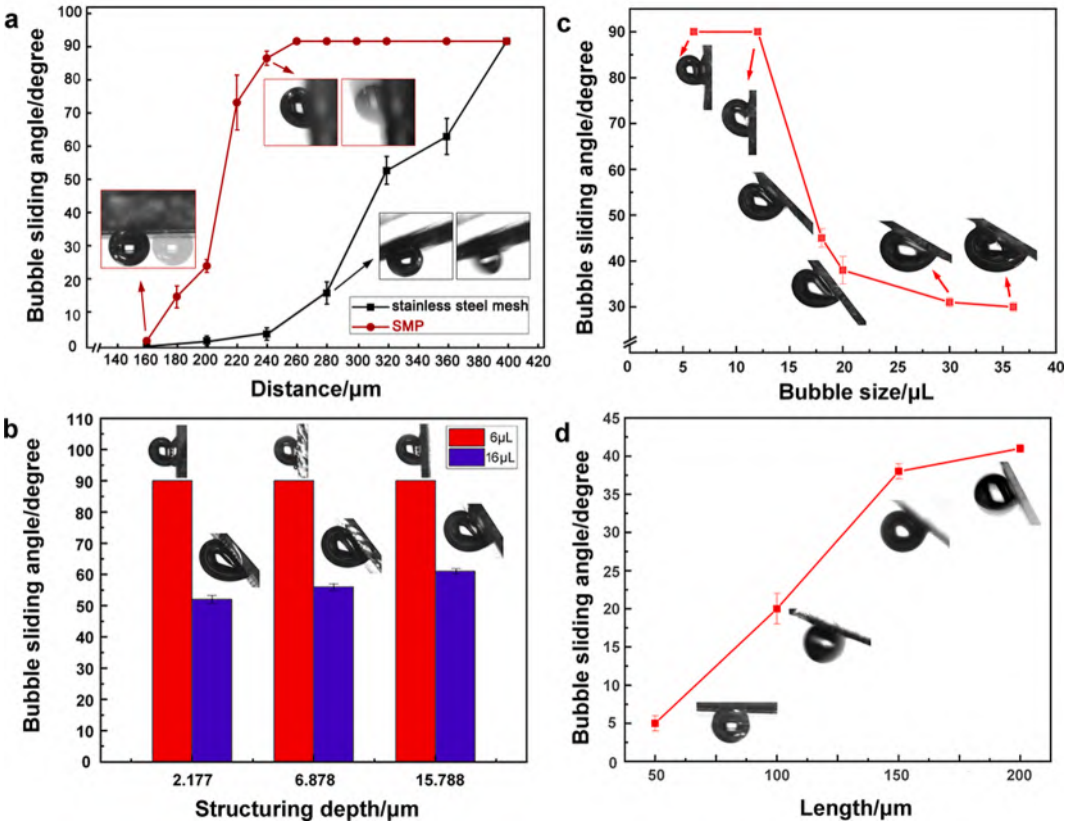

Fig. 3. (a) The relationship between the *BSA* on as-prepared SMP surface with *L* equals 80 μm and increasing *D* (red line), and the *BSA* on laser-induced stainless steel mesh with *L* equals 80 μm and increasing *D* (black line). (b) The relationship between the *BSA* and structuring depth. (c) The relationship between the *BSA* and bubble size. (d) The relationship between the *BSA* and *L* based on same *D*.

sample), and the size of the rough region (using 50/100-patterned, 150/100-patterned, 250/100-patterned, 350/100-patterned SMP samples) to the *BSA* in Fig. 3(b–d). The results showed that the depth of the square rough regions could hardly affect the adhesion regulation. With the increase of the bubble size from 6 μL to 36 μL, the *BSA* decreased gradually indicating a lower bubble adhesion. For the same value of *D*, a smaller *L* owned a lower bubble adhesion. It is because the smaller *L* caused more discontinuous TCL between an underwater bubble and SMP surface, resulting in a smaller barrier for bubble to break through and roll down.

The mechanism of tunable bubble adhesion on the as-prepared surface is discussed below (Fig. 4a-c). The planar SMP domain showed underwater aerophobicity with *SHA* property. The bubble could entirely contact the surface with the successive three-phase contact line (*TCL*) at gas/solid/liquid interface. This contact state could be regarded as the bubble/solid Young's state [8]. For the laser-structured domain, the one-step laser ablation reconstructed the morphology of SMP surface to form the micro/nanostructures without changing the surface chemical composition. Water thoroughly wet the surface and was trapped among the space of microstructures. The bubble could only touch the tip of the microstructures and resulted in an inconsecutive *TCL*. The structured domain surface showed underwater aerophobicity with *SLA* property. This contact state could be regarded as the bubble/solid Cassie/Baxter contact state [8]. When pressing the bubble on the square-patterned array surface downward using a microinjection, the bubble *TCL* was cut by the rough square into several pieces (Fig. 4a, b). In the meanwhile, the part sat on the structured domain (dark yellow color in Fig. 4a) has *SLA*. After releasing the bubble, the recover force would drive the *TCL* fragment move till the *TCL* merged into a complete circle (Fig. 4b). While *L* was set as a constant, the larger value of *D* would directly result in the larger area of the contact circle, accordingly an increasing bubble adhesion force of the surface. As the value of *D* was relatively small, the splutters generated by laser processing piled on the orthogonal center of the four squares, giving rise to the nanoscope structures on the center area. Increasing the *D*, the splutters were more easily covered on the marginal area of rough square domain not the center area. The adhesion of center area increased with *D*, and the center area would not drag bubble down from the microinjection until the *D* is large enough.

The mechanism of bubble sliding process on the squared-patterned array SMP surface is shown in Fig. 4d. When the surface was placed horizontally, the BCA at front *TCL* (dotted line with pink color) and rear *TCL* (dotted line with blue color) maintains the same. Once the surface was tilted, the bubble had upward buoyancy force (F_b), downward y-component adhesion force (F_{ay}), downward y-component support force (F_{Ny}), leftward x-component adhesion force (F_{ax}), and rightward x-component support force (F_{Nx}). With the tilted angle increasing, the top of the bubble deformed and the rear *TCL* retracted due to the continuous rear BCA decrease, which resulting in the detachment of the bubble from planar domain. When the bubble completely detached from the tilted SMP surface, it rolled away rapidly with the protection of wrapped water layer before the layer rupturing.

3.3. Bubble lossless transportation

Microoperation of underwater bubble is of great importance in the drug delivery, cell engineering, and microfluidic fields. Here we used the as-prepared samples with different adhesions to realize the bubble picking and bubble site-specific release in water environment. The 80/240-patterned sample was regarded as the "mechanical hand" to pick up a bubble. Fig. 5a showed that the 80/240-patterned sample took a 7 μL bubble down from the lower surface of 80/80-patterned sample, and moved to the surface of 80/320-patterned sample to realize the bubble lossless horizontal transportation. In this test, the 80/80-patterned sample and the 80/320-patterned sample were fixed face down, while the 80/240-patterned sample served as a "mechanical hand" was drivable with structure surface face up. Firstly, move the "mechanical hand" up to contact the bubble that had been already placed on the *SLA* surface. The "mechanical hand" could pick the bubble up without any

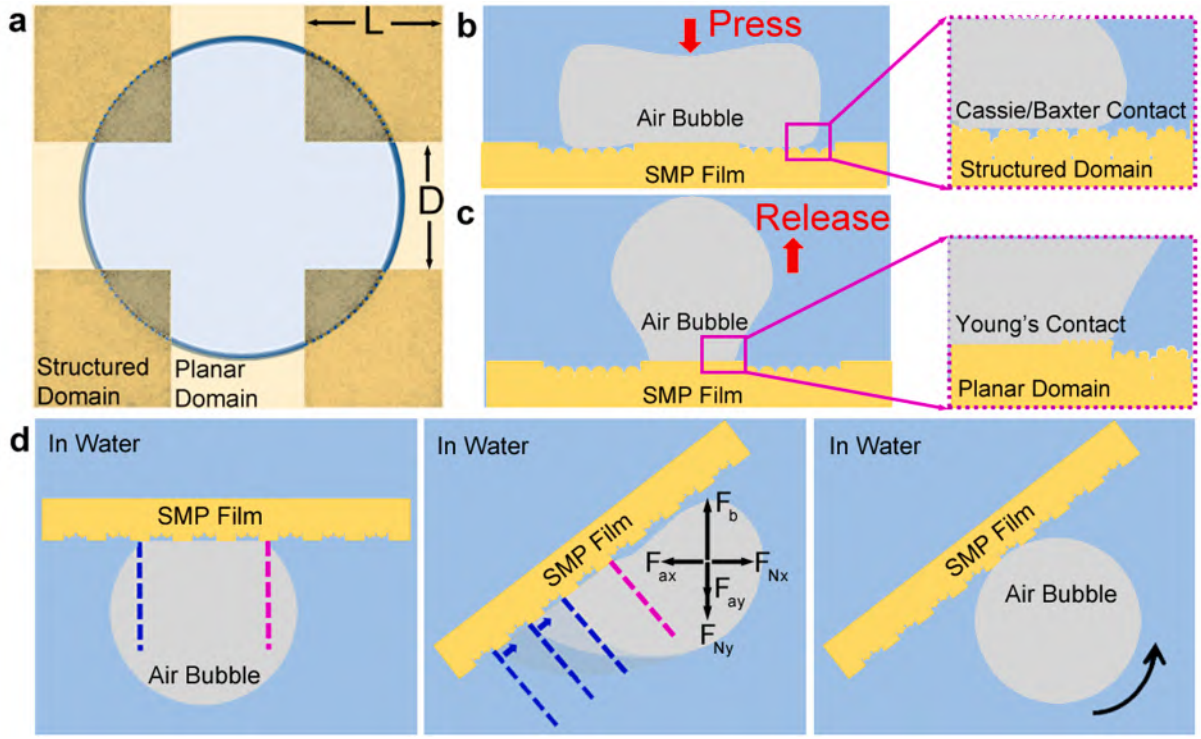

Fig. 4. (a–c) Schematic illustration of the contact model of an underwater bubble on the squared-patterned array SMP surface including planar domain and structured domain: (a) top view, (b) section view when pressing bubble, (c) section view when releasing bubble. (d) Schematic illustration of *BCA* and *BSA* on the face-down squared-patterned array SMP surface.

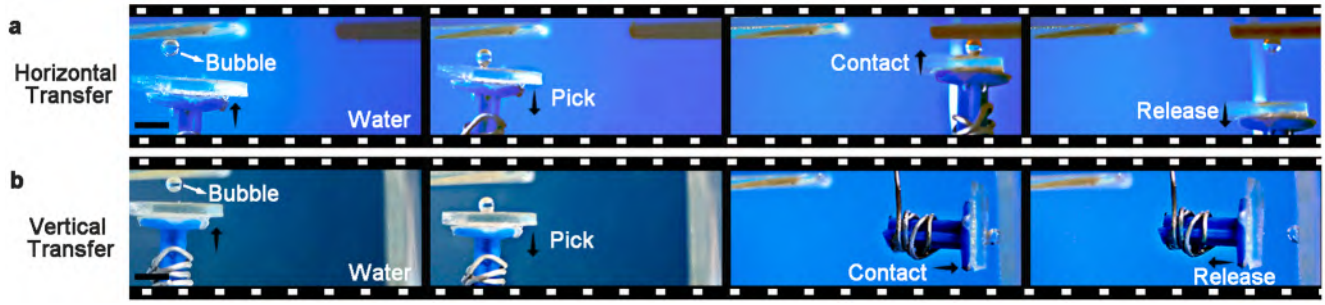

Fig. 5. The 80/240-patterned array SMP film is regarded as "mechanical hand" to realize bubble underwater transportation in horizontal direction (a) and vertical direction (b). The scale bars in (a) and (b) are 4.5 mm.

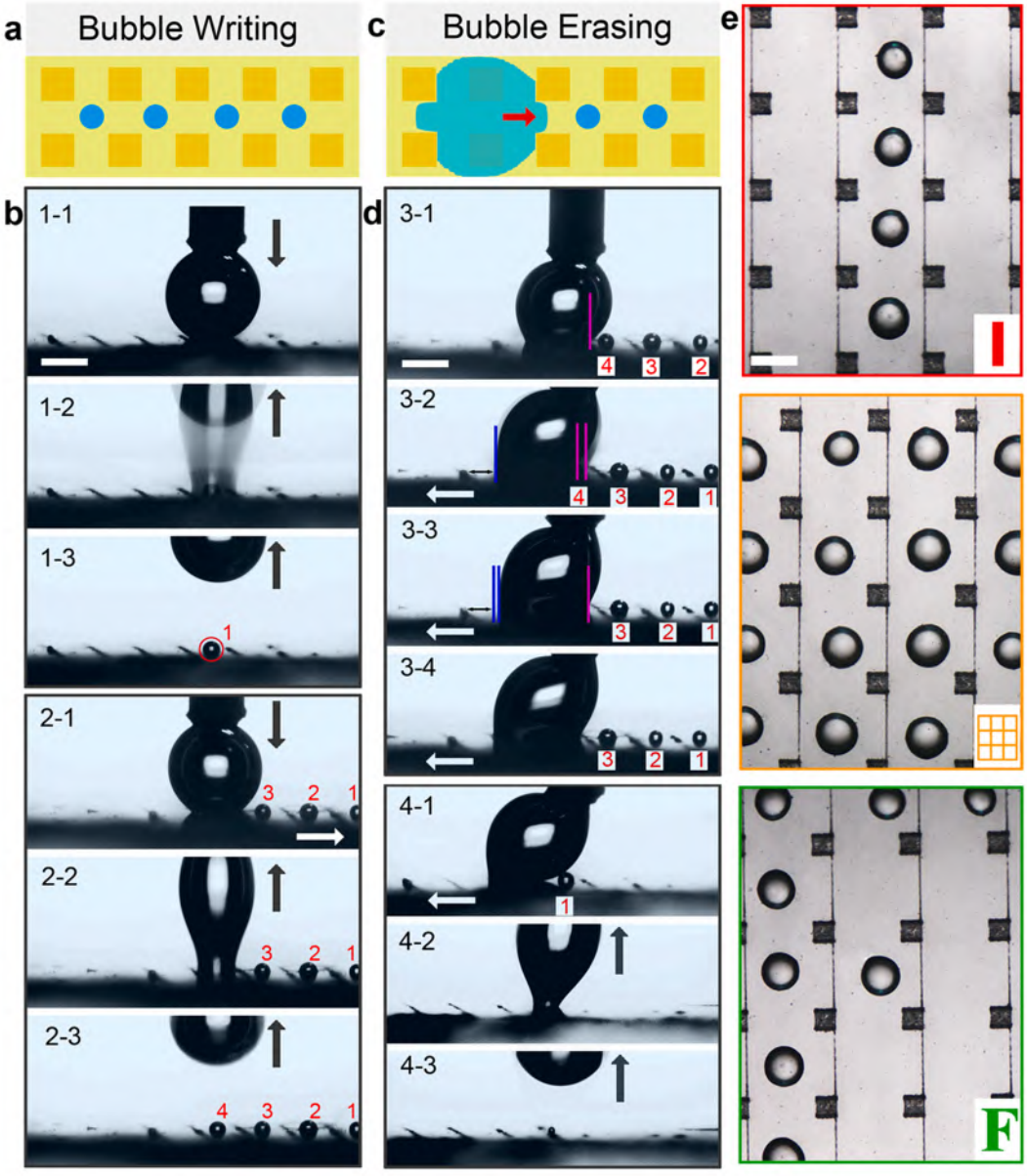

Fig. 6. A programmable tiny-bubble gripping device depending on 80/320-patterned array SMP surface. (a, c) Schematic illustration of tiny bubble writing and erasing. (b) Photo sequence of tiny bubble writing when pressing-lifting a bubble vertically. (d) Photo sequence of tiny bubble erasing when dragging a bubble horizontally. (e) The formation of tiny bubble line, tiny bubble matrix, and tiny bubble pattern. The scale bars in (b), (d) and (e) are 500 μm, 500 μm and 200 μm, respectively.

residual on the *SLA* surface due to its higher adhesion. Next, the bubble could be moved in all directions through taking the "machanical hand" as a carrier. Then, move the bubble up to contact with the *SHA* surface. The bubble was transfered from the "machanical hand" to the *SHA* surface due to its ultra-high adhesion, without any residual on the "machanical hand". The fixing and driving state of any sample could be selective to make the device more flexible. The site-specific bubble transportation could be not limited by the transferring distance and directions. The "mechanical hand" could also transfer an underwater bubble to a vertically placed sample with *L/D* equals to 80/400 (Fig. 5b). Fig. S4 demonstrated the details of the underwater bubble lossless transportation process. We believe that the underwater bubble transportation system will provide application prospects in underwater bubble coalescence, underwater gas microreaction, drug delivery, etc.

3.4. Programmable tiny-bubble gripping device

The as-prepared sample with *HA* property (80/320-patterned sample) could be used to grip tiny bubbles splitting from a "big" bubble and then be erased the tiny bubbles clean. A 0.5 μL bubble was fixed above the 80/320-patterned film and could be moved in the vertical plane, while the film was mobile in the horizontal plane. When the bubble was pressed on the 80/320-patterned sample surface and then lifted up, a tiny bubble left on the surface.

It is because the bubble could only "wet" the planar domain rather than the laser-structured domain when being pressed. During the lifting bubble process, bubble/solid contact area decreased gradually until the area only contained the planar domain. Continuing lifting up, the bubble split on the contact surface, and left a tiny bubble on the sample under the action of the surface adhesion force. Moving the sample at X or Y direction could form various tiny bubble array. Here, for the sake of observation, we generated the tiny bubbles on the planar domain line and placed them in the "one" glyph (Fig. 6a, b).

In addition, re-pressing the "big" bubble onto the tiny bubble on the surface and moving the sample along the "one-glyph" bubble line, tiny bubbles could blend into the "big" bubble again (Fig. 6c, d). The surface of the sample restored clean and could be rewrited tiny bubbles array again. The mechanism of erasing process is ascribed to the evolution of *TCL* of the "big" bubble. Firstly, when the bubble was dragged by the moving surface, the bubble deformed and the *BCA* at the front *TCL* increased. Once the *BCA* was large enough to conquer the free energy barrier (*FEB*) between the planar domain and structured domain, the front *TCL* jumped to next planar domain which resulted in blending of two bubbles (dotted line with carmine color in Fig. 6d). At this moment, the rear *TCL* pinned on and the *BCA* at the rear *TCL* decreased. Later on, along with the sample moving, the rear *TCL* also conquered the *FEB* and jumped with the front *TCL* keeping pinning on (dotted line with blue color in Fig. 6d). Subsequently, after the bubble sliding a small step on planar domain, the jumping-pinning procedure of front and rear *TCL* occurred again to mix next tiny bubble, which ran in cycles until cleaning up all the tiny bubbles. Fig. 6e showed the tiny bubble line, tiny bubble matrix and tiny bubble pattern forming on the 80/320-patterned SMP surface. The programmable tiny-bubble gripping and erasing device was enable applications of research on microbubble/liquid interface, formation of underwater bubble matrix, underwater microreactor and et al.

3.5. In-situ bubble release—macroscopic deformation and recovering

Taking advantages of the excellent macroscopic shape-memory effect of the as-prepared square-patterned SMP film, the bubble adhering and in-situ releasing were realized in water environment under thermal response. The phase state of the fabricated epoxy-based SMP used in this experiment could change from glassy state to rubbery state when the temperature reached to its glass transition temperature Tg (≈55 °C) [41]. The sample was easy to artificially deform ascribed to the storage modulus decreasing greatly. Once the sample was cooling down in a room temperature, it would be glassy state again and maintain the deformation. After re-heating the SMP sample at Tg, it could also turn into the rubbery state and recover to the original shape without man-made operation. Keeping the temperature down, the sample converted to glassy state at original shape where is difficulty to be deformed [39–41].

First off, the 80/220-patterned SMP film was folded in half under the temperature of 55 °C in water. After that, the folded sample was placed into a reservoir full of water at room temperature. In the area where the curvature is the greatest (folding area), the planar domain was stretched and provided a larger high adhesion region for bubbles to pin on. Three bubbles were squeezed and adhered tightly onto the folding area on account of the area stretching. Later, the water in the reservoir was heated by an electromagnetic induction heating device. As illustrated in Fig. 7a, b, with the water temperature rising, the folded sample was recovered gradually to its original shape. The stretched region was also recovered and the stretched area reduced by degrees. When the adhesion force resulted from this region decreased to be indefensible of the bubble buoyancy, the bubble would detach from the sample surface and be in-situ released. As shown in Fig. 7b, the three bubbles were released one by one along with the increase of the water temperature. The water temperature of the space that was close to the electromagnetic induction bar increased faster, therefore the sample in that space was the first to recover leading to the bubble detaching firstly. In the area far away from the electromagnetic bar, the slower water temperature rising velocity resulted in the bubble there the last release.

3.6. Bubble adhesion transition reversely—microscopic deformation and recovering

The microscopic SMP structure was also endowed with the shape-memory effect, which was used to adjust underwater bubble adhesion on the same film that switched reversely between ultralow adhesion and high adhesion. The periodic micro-cone array fabricated by one-step femtosecond laser scanning was shown in Fig. S5. The 3D confocal microscopy image of the laser-induced periodic micro-cone array was shown in Fig. 8a. The periodic interval of the micro-cone array is about 130 μm, and the height of the micro-cone is about 50 μm. There are a myriad of micro/nanoscale protrusions distributing on every micro-cone (Fig. 8c), which is ascribed to the resolidification of ejected particles. Fig. 8b illustrated the surface morphology and bubble adhesion transition process. Immersing the sample into water facedown and placing a 7 μL bubble on it, the bubble could easily roll away with the *BSA* measured of 3° (inset image of Fig. 8c). It is because that the bubble only touched the tips of the nanostructures, and the adhesion of water/solid composite surface is ultralow. Whereafter, applying a slanting shear force by a load and flat glass sheet in hot water at 55 °C and then cooling down, the roof of every micro-cone was flattened and was regarded as a planar surface (Fig. 8c). The deformation of the shape of micro-cone array increase the bubble/solid contact area and decrease the bubble/water contact area, thus the adhesion of the deformed sample was increase accordingly. The *BSA* was measure to be 43° (inset image of Fig. 8c). After reheating the deformed sample in water at 55 °C for about 5 s, the flattened micro-cone was recovered to the original morphology. The tip structure of every micro-cone was also recovered to be hierarchical rough comparing to the pressing flat surface. In this case, the wettability of the SMP surface was also restored with the *BSA* equaling to 6°, revealing an ultralow surface adhesion. Fig. 8d, e showed the 3D confocal microscopy image of the original and deformed periodic micro-cone array from upward view at 45°. It demonstrated that all the pressed micro-cones were flattened uniformly. This bubble adhesion reverse transition process could be operated for at least 10 cycles (Fig. 8f). When increasing the pressing force on the original micro-cone SMP surface at 55 °C, the bubble could pin on the deformed region without releasing even if the surface was faced up. Fig. S6 showed the four words of

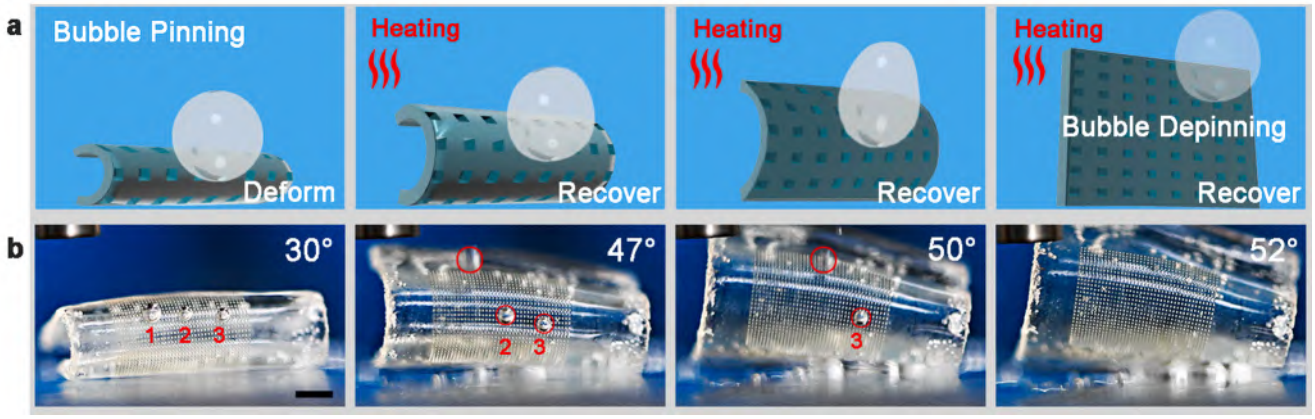

Fig. 7. The schematic illustration (a) and photo sequence (b) of in-situ bubble release taking advantage of shape memory characteristic of SMP film. The bubbles pinned on the folded SMP surface at low water temperature. Heating up the water, the folded SMP film recovered from left to right, and the bubble in-situ released one-by-one in same order. The scale bar in (b) is 250 μm.

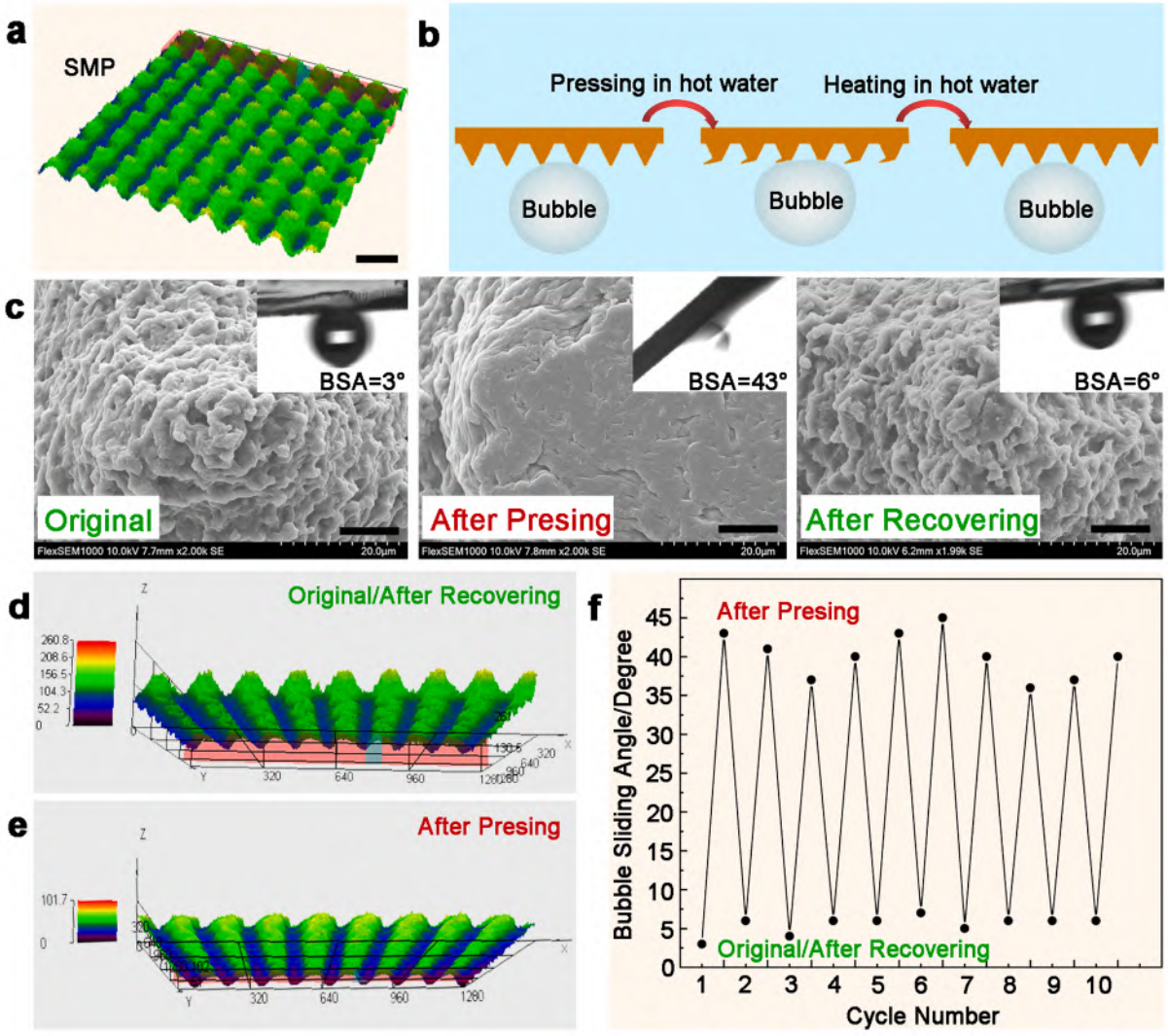

Fig. 8. (a) The 3D confocal microscopy image of the laser-textured periodic micro-cone array. (b) Schematic depiction of the reversible sample morphology and bubble behavior transition between original SMP micro-cone array and deformed micro-cone array. (c) SEM of the original SMP micro-cone array, the micro-cone array after pressing, and the recovered micro-cone array. The inset image is the *BSA* on relevant surface. (d, e) The 3D confocal microscopy images of original and deformed micro-cone array from upward view at 45°. (f) The reversible transition could be operated for several cycles. The scale bars in (a) and (c) are 150 μm and 10 μm.

"XJTU" bubble pattern in the pressed region.

4. Conclusions

In conclusion, we proposed four types of bubble adhesion states on solid surface and realized multi-manipulation of bubbles in aqueous environment using femtosecond laser-induced square-patterned array SMP surface. By adjusting the value of *L* and *D* of the as-prepared sample, the *BSA* could be changed from 0° to 90° indicating the bubble adhesion on samples varied from ultralow to ultrahigh. The *LA* surface was considered as "mechanical hand" to transfer a bubble losslessly from *SLA* surface to *HA* surface horizontally and *SHA* surface vertically. The *HA* surface with *L* of 80 μm and *D* of 320 μm was regarded as a programmable tiny-bubble gripping device to form microbubble pattern that could be erased and rewrited. Taking advantages of excellent macroscopic and microscopic shape-memory property of SMP film, the in-situ bubble release and reversely transition of bubble adhesion between ultralow and high were completed. This work provided a new strategy to manipulate underwater bubbles based on solid adhesion and a potential in the fields of medical and microfluidic

Declaration of Competing Interest

The authors declare that they have no known competing financial interests or personal relationships that could have appeared to influence the work reported in this paper.

Acknowledgments

This work is supported by the National Science Foundation of China under the Grant nos. 61875158, the National Key Research and Development Program of China under the Grant no. 2017YFB1104700, the International Joint Research Laboratory for Micro/Nano Manufacturing and Measurement Technologies, the Fundamental Research Funds for the Central Universities.

Appendix A. Supplementary data

Supplementary data to this article can be found online at https://doi.org/10.1016/j.cej.2021.128694.

References

[1] P. Marmottant, S. Hilgenfeldt, Controlled vesicle deformation and lysis by single oscillating bubble, Nature 423 (2003) 153–156.
[2] K. Ferrara, R. Pollard, M. Borden, Ultrasound microbubble contrast agents: fundamentals and application to gene and drug delivery, Annu. Rev. Biomed. Eng. 9 (2007) 415–447.
[3] G.N. Sankin, F. Yuan, P. Zhong, Pulsating tandem microbubble for localized and directional single-cell membrane poration, Phys. Rev. Lett. 105 (7) (2010), https://doi.org/10.1103/PhysRevLett.105.078101.
[4] S. Jin, X. Wei, Z. Yu, J. Ren, Z. Meng, Z. Jiang, Acoustic-controlled bubble generation and fabrication of 3D polymer porous materials, ACS Appl. Mater. Interfaces 12 (2020) 22318–22326.
[5] X. Zuo, K. Chang, J. Zhao, Z. Xie, H. Tang, B. Li, Z. Chang, Bubble-template-assisted synthesis of hollow fullerene-like MoS2 nanocages as a lithium ion battery anode material, J. Mater. Chem. A 4 (2016) 51–58.
[6] K. Szla, M. Costantini, J. Jaroszewicz, L. Kozon, S. Wojciech, P. Garstecki, C. Stubenrauch, A. Barbetta, J. Guzowski, 3D-printing of functionally graded porous materials using on-demond reconfigurable microfluidics, Angew. Chem. Int. Ed. 58 (2019) 7620–7625.
[7] Z. Huang, S. Zhao, M. Su, Q. Yang, Z. Li, Z. Cai, H. Zhao, X. Hu, H. Zhou, F. Li, J. Yang, Y. Wang, Y. Song, Bioinspired patterned bubbles for broad and low-frequency acoustic blocking, ACS Appl. Mater. Interfaces 12 (2020) 1757–1764.
[8] J. Yong, F. Chen, Y. Fang, J. Huo, Q. Yang, J. Zhang, H. Bian, X. Hou, Bioinspired design of underwater superaerophobic and superaerophilic surfaces by femtosecond laser ablation for anti- or capturing bubbles, ACS Appl. Mater. Interfaces 9 (45) (2017) 39863–39871.
[9] C. Shi, X. Cui, X. Zhang, P. Tchoukov, Q. Liu, N. Encinas, M. Paven, F. Geyer, D. Vollmer, Z. Xu, H. Butt, H. Zeng, Interaction between air bubble and superhydrophobic surfaces in aqueous solutions, Langmuir 31 (2015) 7317–7327.
[10] J. Yong, F. Chen, M. Li, Q. Yang, Y. Fang, J. Huo, X. Hou, Remarkably simple achievement of superhydrophobicity, superhydrophilicity, underwater superoleophobicity, underwater superoleophilicity, underwater superaerophobicity, and underwater superaerophilicity on femtosecond laser ablated PDMS surfaces, J. Mater. Chem. A 5 (48) (2017) 25249–25257.
[11] C. Yu, P. Zhang, J. Wang, L. Jiang, Superwettability of gas bubbles and its application: from bioinspiration to advanced materials, Adv. Mater. 29 (45) (2017) 1703053, https://doi.org/10.1002/adma.201703053.
[12] C. Huang, Z. Guo, The wettability of gas bubble: from macro behavior to nano structures to applications, Nanoscale 10 (2018) 19659–19672.
[13] J. Yong, F. Chen, J. Huo, Y. Fang, Q. Yang, J. Zhang, X. Hou, Femtosecond laser induced underwater superaerophilic and superaerophobic PDMS sheet with through-microholes for air bubbles selectively passing through and further collecting underwater gas, Nanoscale 10 (2018) 3688–3696.
[14] J. Li, Z. Guo, Bubble shapes and their changes on slippery surfaces during directional transportation, J. Colloid Interf. Sci. 552 (2019) 84–90.
[15] J.E. George, S. Chidangil, S.D. George, Recent progress in fabricating superaerophobic and superaerophilic surfaces, Adv. Mater. Interfaces 4 (9) (2017) 1601088, https://doi.org/10.1002/admi.201601088.
[16] C. Yu, X. Zhu, M. Cao, C. Yu, K. Li, L. Jiang, Superhydrophobic helix: controllable and directional bubble transport in an aqueous environment, J. Mater. Chem. A 4 (43) (2016) 16865–16870.
[17] C. Yu, M. Cao. Z. Dong, J. Wang, K. Li, L. Jiang, Spontaneous and directional transportation of gas bubbles on superhydrophobic cones, Adv. Funct. Mater. 26 (2016) 3236–3243.
[18] H. Ma, M. Cao, C. Zhang, Z. Bei, K. Li, C. Yu, L. Jiang, Directional and continuous transport of gas bubbles on superaerophilic geometry-gradient surfaces in aqueous environments, Adv. Funct. Mater. 28 (7) (2018) 1705091, https://doi.org/10.1002/adfm.v28.710.1002/adfm.201705091.
[19] C. Chen, Z. Huang, L. Shi, Y. Jiao, S. Zhu, J. Li, Y. Hu, J. Chu, D. Wu, L. Jiang, Remote photothermal actuation of underwater bubble towards arbitrary direction on planar slippery Fe_3O_4-doped surfaces, Adv. Funct. Mater. 29 (2019) 1904766.
[20] S. Zhu, Y. Bian, T. Wu, C. Chen, Y. Jiao, Z. Jiang, Z. Huang, E. Li, J. Li, J. Chu, Y. Hu, D. Wu, L. Jiang, High performance bubble manipulation on ferrofluid-infused laser-ablated microstructured surfaces, Nano Lett. 20 (2020) 5513–5521.
[21] C. Chen, Z. Huang, Y. Jiao, Y. Zhang, J. Li, C. Li, X. Lv, S. Wu, Y. Hu, W. Zhu, D. Wu, J. Chu, L. Jiang, In-situ reversible control between sliding and pinning for diverse liquids under ultralow voltage, ACS Nano 13 (2019) 5742–5752.
[22] P. Zhang, J. Zhang, Z. Xue, J. Wang, L. Jiang, Reliable manipulation of gas bubble by regulating interfacial morphologies and chemical components, Mater. Horiz. 4 (2017) 665–672.
[23] X. Lv, Y. Jiao, S. Wu, C. Li, Y. Zhang, J. Li, Y. Hu, D. Wu, Anisotropic sliding of underwater bubbles on micro-grooved slippery surfaces by one-step femtosecond laser scanning, ACS Appl. Mater. Interfaces 11 (2019) 20574–20580.
[24] Y. Jiao, X. Lv, Y. Zhang, C. Li, J. Li, H. Wu, Y. Xiao, S. Wu, Y. Hu, D. Wu, J. Chu, Pitcher plant bioinspired bubble slippery surface fabricated by femtosecond laser for buoyancy-driven gas self-transport and efficient capture, Nanoscale 11 (2019) 1370–1378.
[25] C. Zhang, B. Zhang, H. Ma, Z. Li, X. Xiao, Y. Zhang, X. Cui, C. Yu, M. Cao, L. Jiang, Bioinspired pressure-tolerant asymmetric slippery surface for continuous self-transport of gas bubbles in aqueous environment, ACS Nano 12 (2018) 2048–2055.
[26] M. Cao, Z. Li, H. Ma, H. Geng, C. Yu, L. Jiang, Is superhydrophobicity equal to underwater superaerophilicity: regulating the gas behavior on superaerophilic surface via hydrophilic defects, ACS Appl. Mater. Interfaces 10 (2018) 20995–21000.
[27] X. Xue, R. Wang, L. Lan, J. Wang, Z. Xue, L. Jiang, Reliable manipulation of gas bubble size on superaerophilic cones in aqueous media, ACS Appl. Mater. Interfaces 10 (2018) 5099–5106.
[28] Q. Li, D. Wu, Z. Guo, Drop/bubble transportation and controllable manipulation on patterned slippery lubricant infused surfaces with tunable wettability, Soft Matter 15 (2019) 6803–6810.
[29] A.n. Li, H. Li, Z. Li, Z. Zhao, K. Li, M. Li, Y. Song, Programmable droplet manipulation by a magnetic-actuated robot, Sci. Adv. 6 (7) (2020) eaay5808, https://doi.org/10.1126/sciadv.aay5808.
[30] P. Tian, X. Gao, G. Wen, L. Zhong, Z. Wang, Z. Guo, Diving-floating locomotion induced by capturing and manipulating bubbles in an aqueous environment, Chem. Commun. 54 (2018) 11713–11716.
[31] J. Wang, Q. Yang, M. Wang, C. Wang, L. Jiang, Rose petals with a novel and steady air bubble pinning effect in aqueous media, Soft Matter 8 (2012) 2261–2266.
[32] Y. Zhang, Y. Li, Y. Hu, X. Zhu, Y. Huang, Z. Zhang, S. Rao, Z. Hu, W. Qiu, Y. Wang, G. Li, L. Yang, J. Li, D. Wu, W. Huang, C. Qiu, J. Chu, Localized self-growth of reconfigurable architectures induced by a femtosecond laser on a shape-memory polymer, Adv. Mater. 30 (49) (2018) 1803072, https://doi.org/10.1002/adma.201803072.
[33] J. Yong, F. Chen, Q. Yang, Z. Jiang, X. Hou, A review of femtosecond-laser-induced underwater superoleophobic surfaces, Adv. Mater. Interfaces 5 (7) (2018) 1701370, https://doi.org/10.1002/admi.201701370.
[34] K. Yin, S. Yang, X. Dong, D. Chu, J.-A. Duan, J. He, Robust laser-structured asymmetrical PTFE mesh for underwater directional transportation and continuous collection of gas bubbles, Appl. Phys. Lett. 112 (24) (2018) 243701, https://doi.org/10.1063/1.5039789.
[35] K. Yin, D. Chu, X. Dong, C. Wang, J. Duan, J. He, Femtosecond laser induced robust periodic nanoripples structured mesh for highly efficient oil-water separation, Nanoscale 9 (2017) 14229–14235.
[36] S. Yang, K. Yin, J. Wu, Z. Wu, D. Chu, J. He, J. Duan, Ultrafast nano-structuring of superwetting Ti foam with robust antifouling and stability towards efficient oil-in-water emulsion separation, Nanoscale 11 (2019) 17607–17614.

[37] H. Lu, Y. Liu, J. Leng, S. Du, Qualitative separation of the physical swelling effect on the recovery behavior of shape memory polymer, Eur. Polym. J. 46 (2010) 1908–1914.
[38] H. Lu, S. Du, A phenomenological thermodynamic model for the chemo-responsive shape memory effect in polymers based on flory-huggins solution theory, Polym. Chem. 5 (2014) 1155–1162.
[39] Z. Cheng, D. Zhang, T. Lv, H. Lai, E. Zhang, H. Kang, Y. Wang, P. Liu, Y. Liu, Y. i. Du, S. Dou, L. Jiang, Superhydrophobic shape memory polymer arrays with switchable isotropic/anisotropic wetting, Adv. Funct. Mater. 28 (7) (2018) 1705002, https://doi.org/10.1002/adfm.201705002.
[40] D. Zhang, Z. Cheng, Y. Liu, Smart wetting control on shape memory polymer surface, Chemistry (2018).
[41] X. Bai, Q. Yang, Y. Fang, J. Yong, Y. Bai, J. Zhang, X. Hou, F. Chen, Anisotropic adhesion-switchable, and thermal-responsive superhydrophobicity on the femtosecond laser-structured shape-memory polymer for droplet manipulation, Chem. Eng. J. 400 (2020) 125930, https://doi.org/10.1016/j.cej.2020.125930.
[42] J. Huo, J. Yong, F. Chen, Q. Yang, Y. Fang, X. Hou, Trapped air-induced reversible transition between underwater superaerophilicity and superaerophobicity on the femtosecond laser-ablated superhydrophobic PTFE surfaces, Adv. Mater. Interfaces 6 (17) (2019) 1900262, https://doi.org/10.1002/admi.201900262.
[43] J. Huo, Q. Yang, J. Yong, P. Fan, Y. Lu, X. Hou, F. Chen, Underwater superaerophobicity/superaerophilicity and unidirectional bubble passage based on the femtosecond laser-structured stainless steel mesh, Adv. Mater. Interfaces 7 (14) (2020) 1902128, https://doi.org/10.1002/admi.v7.1410.1002/admi.201902128.